

Active Nanocomposites:
**Energy Harvesting and Stress Generation Media for Future
Multifunctional Aerospace Structures**

Final Technical Report

Investigators:

Zoubeida Ounaies, Aerospace Engineering, Texas A&M University

Ramanan Krishnamoorti, Chemical Engineering, University of Houston

Richard Vaia, Materials and Manufacturing Directorate, AFRL/MLBP

To: **Dr. Les Lee**

Contract/Grant #: **FA9550-06-1-0422**

Report Documentation Page			Form Approved OMB No. 0704-0188		
Public reporting burden for the collection of information is estimated to average 1 hour per response, including the time for reviewing instructions, searching existing data sources, gathering and maintaining the data needed, and completing and reviewing the collection of information. Send comments regarding this burden estimate or any other aspect of this collection of information, including suggestions for reducing this burden, to Washington Headquarters Services, Directorate for Information Operations and Reports, 1215 Jefferson Davis Highway, Suite 1204, Arlington VA 22202-4302. Respondents should be aware that notwithstanding any other provision of law, no person shall be subject to a penalty for failing to comply with a collection of information if it does not display a currently valid OMB control number.					
1. REPORT DATE 30 JUN 2010		2. REPORT TYPE Final		3. DATES COVERED 01-06-2006 to 30-11-2009	
4. TITLE AND SUBTITLE ACTIVE NANOCOMPOSITES: ENERGY HARVESTING AND STRESS GENERATION MEDIA FOR FUTURE MULTIFUNCTIONAL AEROSPACE STRUCTURES			5a. CONTRACT NUMBER FA9550-06-1-0422		
			5b. GRANT NUMBER		
			5c. PROGRAM ELEMENT NUMBER		
6. AUTHOR(S) Zoubaida Ounaies			5d. PROJECT NUMBER		
			5e. TASK NUMBER		
			5f. WORK UNIT NUMBER		
7. PERFORMING ORGANIZATION NAME(S) AND ADDRESS(ES) TEXAS ENGINEERING EXPERIMENT STATION,DEPT OF AEROSPACE ENGINEERING/736B H. R. BRIGHT BUILDING,3141 TAMU,College Station,TX,77843			8. PERFORMING ORGANIZATION REPORT NUMBER ; AFRL-OSR-VA-TR-2011-0239		
9. SPONSORING/MONITORING AGENCY NAME(S) AND ADDRESS(ES) AFOSR, 875 North Randolph Street, Suite 325, Arlington, VA, 22203			10. SPONSOR/MONITOR'S ACRONYM(S)		
			11. SPONSOR/MONITOR'S REPORT NUMBER(S) AFRL-OSR-VA-TR-2011-0239		
12. DISTRIBUTION/AVAILABILITY STATEMENT Approved for public release; distribution unlimited					
13. SUPPLEMENTARY NOTES					
14. ABSTRACT The program successfully demonstrated experimental evidence of the creation of an electrostrictive response in amorphous polymer nanocomposites by addition of small quantities of nanoparticles. Further, it has been also verified that their piezoelectric response can be dramatically enhanced through addition of conductive nanoparticles, such as carbon nanotubes without additional weight penalties. Most importantly, these improvements were achieved at much lower actuation voltages, and were accompanied by increase in both mechanical and dielectric properties. The efforts reported provide new avenues to significantly improve the electromechanical response of EAP-based nanocomposites.					
15. SUBJECT TERMS					
16. SECURITY CLASSIFICATION OF:			17. LIMITATION OF ABSTRACT Same as Report (SAR)	18. NUMBER OF PAGES 30	19a. NAME OF RESPONSIBLE PERSON
a. REPORT unclassified	b. ABSTRACT unclassified	c. THIS PAGE unclassified			

Contents

Executive Summary	3
I. Introduction	4
II. Experimental Approach	5
A. <i>Polyimide-based nanocomposites:</i>	5
B. <i>PVDF-based nanocomposites:</i>	6
III. Results.....	7
A. <i>Polyimide nanocomposite actuators as electrostrictors:</i>	7
B. <i>PVDF nanocomposite actuators as electrostrictors:</i>	16
C. <i>Probing mechanism of electrostriction:</i>	17
D. <i>Summary of significant findings</i>	23
IV. DURIP Equipment-Enabled Research	23
A. <i>Nano-indentation</i>	23
B. <i>Raman spectroscopy</i>	25
C. <i>In-situ Raman combined with mechanical tests</i>	25
D. <i>In-situ Raman spectroscopy/nano-indentation experiments</i>	26
E. <i>Experimental procedure</i>	27
F. <i>Results and discussion</i>	27
V. Remaining Challenges	28

Executive Summary

Electric field-activated electroactive polymers (EAPs) are an attractive class of smart materials that exhibit electromechanical coupling conversion; hence they can be applied as solid-state actuators and motion or pressure sensors. These EAPs have many advantages compared to other classes of materials. They are lightweight, shape conformable, generally have good energy densities, relatively high strain rates, good electromechanical coupling and high bandwidth. However, there are major obstacles to their transition to applications. Notably they require high actuation voltages, have low blocked stresses and low operating temperatures. These current limitations are linked to inherent polymer properties such as low dielectric constant and low modulus. In this project, our goals were to develop the science and necessary technology surrounding active nanostructured hybrid composites to provide new polymer-based material systems that exhibit enhanced actuation/sensing and 10-20 times the energy harvesting performance of current polymeric materials. To achieve this goal the nanoparticles will be used simultaneously as structural reinforcement **and** to enhance electromechanical coupled response and distributed sensing. This is the key concept and aspect of the proposed research that is unique and distinct from other nano-composite programs. The system and associated processing requirements will be provided by AFRL/VA and our industrial partners, thus ensuring rapid focus of the materials development program within the context of the necessary structural configuration.

We have successfully demonstrated experimental evidence of the creation of an electrostrictive response in amorphous polymer nanocomposites by addition of small quantities of nanoparticles. Further, we have also verified that their piezoelectric response can be dramatically enhanced through addition of conductive nanoparticles, such as carbon nanotubes without additional weight penalties. Most importantly, these improvements were achieved at much lower actuation voltages, and were accompanied by increase in both mechanical and dielectric properties. Our efforts reported herein provide new avenues to significantly improve the electromechanical response of EAP-based nanocomposites.

The fabrication of electroactive polymer-based materials with sensing and actuation capabilities will make significant contributions towards the development and integration of adaptive, active and smart materials for air and space vehicles, including those in deployable aerospace structures, unmanned aerial vehicles, robotics, ultra-small micro-air vehicles and smart textiles. The combination of properties promised by polymer nanocomposites provides opportunities for going beyond structural reinforcement where engineered electroactive responses and enhanced electrical and dielectric properties would result in multifunctionality.

We have collaborated very closely with AFRL researchers, namely the co-PI Richard Vaia and his group. This collaboration generated output beyond research results, in that we co-wrote conference proceedings and a journal manuscript, we co-organized sessions in international conferences, we co-presented oral papers and posters together and we had an exchange of students and postdoc visits.

I. Introduction

Incorporating carbon nanotubes (CNTs) in polymers offers a means of exploiting their superior mechanical [1] and electrical properties [2]. Although enhancements in properties have been shown for structural applications [3,4] and for electrostatic discharge [5], there have been fewer investigations on these nanocomposites as actuator materials. Some researchers have probed the electromechanical properties of individual or bundles of CNTs. Roth et al. investigated single walled carbon nanotubes (SWNTs) as actuators using an atomic force microscope, and found that the SWNTs exhibit an electromechanical coupling [6]. They observed a change in the length of the SWNT due to weakened carbon-carbon bonds, resulting from injection of electrons. In a separate study, Baughman et al. investigated actuation of SWNT sheets, or Bucky paper, in an electrolyte [7]. The actuation was electro-chemically driven, where a macroscopic bending displacement of the sheets was seen in a bimorph cantilever configuration. El-Hami et al. used an AFM tip to apply a voltage across an aligned bundle of SWNTs, and observed a thickness expansion as a result [8]. They concluded that the nanotubes possessed an electrostrictive nature. Similarly, Guo et al. predicted an axial electrostrictive response in SWNTs using density functional quantum mechanics calculations [9].

Other investigations have focused on the effect of CNTs on the electromechanical response of polymers. Kang et al. have demonstrated an enhancement in the response of a piezoelectric polyimide, (β -CN) APB-ODPA, in the presence of SWNTs [10]. They investigated a series of poled SWNT-polyimide composites and quantified their piezoelectric response through Thermally Stimulated Current (TSC) analysis as well as by direct measurement of the in-plane piezoelectric strain coefficient, d_{31} . In general, they observed an increase in d_{31} normalized by poling voltage from a value of 1 for pure polyimide to 1.2 for polyimide with 0.02 wt% SWNT content. Levi et al. have demonstrated an increase in the piezoelectric properties of poly(vinylidene fluoridetrifluoroethylene) (PVDF-TrFE) due to SWNTs. The researchers observed an increase in the d_{31} value from 20 pC/N for the pure polymer film to 25 pC/N for 0.1wt% SWNT content composite. This enhancement has been attributed to an increase in the piezoelectric β -phase due to addition of SWNTs [11]. Effect of multiwalled carbon nanotubes (MWNTs) on the actuation stress response of a polysiloxane nematic elastomers has been studied [12]. The elastomer without MWNTs did not show any actuation stress, while an increased stress response was seen in the 0.0085wt% and 0.02wt% MWNT composites under an applied electric field. The actuation was attributed to the torque experienced by the nanotubes due to the applied field. Similarly, in a study involving ionic polymer metal composites (IPMCs), an enhancement in the actuation stress was observed for 1wt% MWNT loading above which a decrease in response is seen due to inhomogeneous distribution of the MWNTs [13]. In a different study, Akle et al. have demonstrated an increase in the strain and strain rate of a hybrid IPMC actuator by incorporating SWNTs in the electrodes, taking advantage of their conductive nature [14]. Zhang et al have demonstrated enhancement in the electrostrictive response of MWNT-poly(vinylidene fluoride-trifluoroethylene-chlorofluoroethylene) composites compared to the pure copolymer, with MWNT content of 0.5wt% and 1wt% [15]. The authors reported an increase in both the mechanical and dielectric properties of these composites, which led to the enhanced strain response at a reduced electric field.

The studies described above used already electroactive polymers as the matrix materials. Consequently, they observed modest increase in piezoelectricity or other electromechanical response already present in the polymer. In addition, the response is not followed by a significant decrease in actuation voltage, which is one important challenge in using current EAPs.

II. Experimental Approach

We focused on two polymer systems: amorphous polyimides and semicrystalline poly(vinylidene fluoride) (PVDF). Below are the processing and characterization methods we have used throughout the project for both systems.

A. Polyimide-based nanocomposites:

SWNTs used are laser-ablated SWNTs acquired from Rice University. Details on aspect ratio, solvent-based dispersion and processing are given in an earlier publication [16]. An aromatic colorless polyimide (PI), CP2 (see chemical structure in Fig. 1) is used as the polymer matrix material. The diamine and dianhydride used to prepare the CP2-PI are 1,3-bis(3-aminophenoxy) benzene (APB) and 2,2-bis (3,4-anhydrodicarboxyphenyl) hexafluoropropane (6FDA). The SWNT-PI composite is solution cast using in-situ polymerization under sonication.

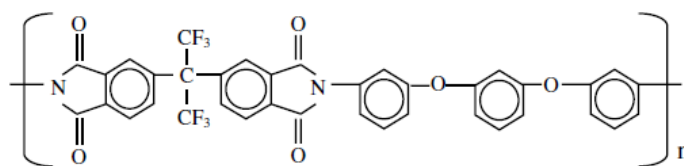


Fig. 1. Chemical structure of CP2 polyimide.

Scanning Electron Microscopy (SEM) images are taken using a Zeiss 1530 high resolution, variable pressure FE SEM. The SWNT-PI composites are freeze-fractured. The conductive coating used for the SEM study is Pt-Pd.

For electrical and electromechanical measurements, the nanocomposite films are coated with a thin silver layer by a vapor deposition process. The thickness of the samples ranges from 30-60 μm , and that of the silver layer is kept at 100nm. A QuadTech 7600 Precision LCR meter is used to measure AC electrical conductivity and dielectric constant of the nanocomposites in a parallel plate configuration over a range of frequencies (20Hz – 1MHz) and SWNT vol% (0,0.05,0.1,0.2,0.5,1,2). A Sun Systems EC1x environmental chamber is used to add temperature capability. The percolation threshold, concentration at which the material behavior changes from insulator to that of a conductor, is obtained from these measurements. The electroded samples are cut into strips of 3cm x 0.5cm, which are then used for the electromechanical tests. Fig. 2 shows the experimental set-ups. For thickness actuation, a small area on the bottom face is constrained and the electric field is applied through the thickness (Fig. 2(a)). The change in thickness is measured by an Opto Acoustics dual channel 201 angstrom resolver. For the bending experiment, the top of the sample is sandwiched between glass plates with copper leads. This setup is then suspended vertically in an acrylic box chamber (Fig. 2(b)). The leads allow the application of electric field (DC or AC) to the strip. The bending of the sample is captured by a Photron Fastcam PCI R2 high speed camera setup. An auxiliary light source is available for better visibility. The captured videos are analyzed using Photron image analysis software. This software allows measurement of the sample displacement by analyzing the sample position in successive video frames. Thermally Stimulated Current (TSC) measurements are carried out using a Setaram TherMold TSC/RMA 9000. The polymer or polymer nanocomposite is poled by DC electric field around the glass transition temperature, T_g . The poling time is 20 minutes and is kept the same for all samples. The sample is then cooled rapidly to room temperature using liquid nitrogen and then

re-heated slowly (2°C/min) to 300°C. The depolarization current is measured during this heating ramp. TSC and dielectric measurements are powerful tools to investigate both the polarization inherent in the polymer and that due to the presence of nanotubes.

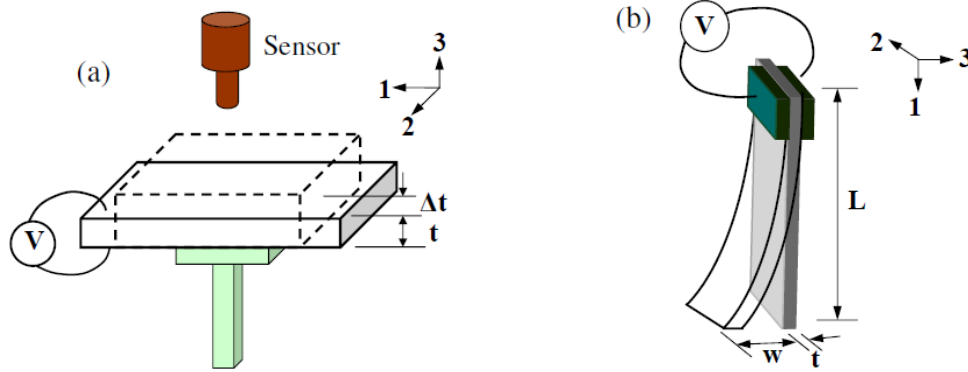


Fig. 2. (a) Thickness actuation, (b) Bending actuation

B. PVDF-based nanocomposites:

PVDF used in this study is KYNAR 301 in powder form. The unpurified HiPCO single walled carbon nanotubes were obtained from Rice University. They were further purified by a process based on [17]. The PVDF-SWNT composites are prepared by a solution casting process. SWNTs are dispersed in N,N-dimethyl acetamide (DMAc) using a probe sonicator for 3 hrs. The KYNAR 301 powder is then added to the solution and mixed using shear mixing by employing a mechanical stirrer in the presence of an 40 kHz ultrasonic bath for 24hrs. The PVDF-SWNT solution is then heated in an oven through 130°C before casting it on glass slide using a doctor blade. The cast film is then kept in the oven at 130°C until all the DMAc evaporates to give a solvent free film. The high temperature is used to ensure low viscosity and DMAc evaporation.

The dried nanocomposite films are coated with a thin silver layer (100nm) by a vapor deposition process. The electrical and dielectric properties of the composites with varying SWNT content are measured using a Novocontrol broadband dielectric spectrometer over the frequency range: 0.01 Hz - 10⁷ Hz. For thickness actuation, a small area on the bottom face of the electroded sample is constrained and the electric field is applied through the thickness t (Figure 2(a)). An MTI 2100 photonic fiber optic sensor is used to measure the change in thickness (Δt). The thickness strains are then calculated as;

$$S_{33} = \frac{\Delta t}{t}$$

The electroded film samples are then cut into strips of 3cm x 0.5cm, which are then used for the bending actuation tests. Figure 2(b) shows the experimental set-up used. The top of the sample is sandwiched between glass slides with copper leads. This setup is then suspended vertically in an fiber-glass box chamber. The leads allow the application of electric field (DC or AC) to the strip. The bending of the sample is captured by a Photron Fastcam PCI R2 high speed camera setup. An auxiliary light source is available for better visibility. The captured videos are analyzed using Photron image analysis software. This software allows measurement of the sample displacement by analyzing the sample position in successive video frames. The longitudinal strains due to bending are computed assuming the sample as a cantilever beam under a constant bending moment. The sample under a uniform radius of curvature would then show longitudinal strains in the outermost layer, S_{11} , as [18];

$$S_{11} = \frac{w \cdot t}{L^2}$$

where w is the tip displacement of the bent samples, t is the thickness and L is the length of the film actuator sample respectively.

The effect of adding SWNTs on the microstructure of PVDF is studied using Fourier transform infrared spectroscopy (FTIR). The FTIR studies are conducted using the Thermo Electron Corporation Nicolet 380 FTIR in the ATR mode. The scanning range employed is 400 cm^{-1} – 4000 cm^{-1} with a resolution of 4 cm^{-1} . Differential scanning calorimetry (DSC) is used to quantify the effect of SWNTs on the crystallinity of PVDF. A TA instruments DSC Q20 is used at a heating rate of $10^\circ\text{C}/\text{min}$. The degree of crystallinity is determined from the endotherm peak area using 104.6 J/g as the heat of fusion of 100% crystalline PVDF [19, 20]. A Nanonics Multiview 1000 Raman spectrometer employing a 532 nm laser is used to probe the interaction between the polymer and SWNTs. A TA instruments Q400 thermo mechanical analyzer (TMA) is used to measure the coefficients of thermal expansion to quantify Joule heating contributions to the measured strain response.

III. Results

A. *Polyimide nanocomposite actuators as electrostrictors:*

Using both Optical Microscopy (OM) and Transmission Electron Microscopy (TEM), we conclude that excellent dispersion was achieved and that optical transparency of the composites remained high until 1 vol% SWNT loading.

The plot of electrical conductivity as a function of SWNT concentration is shown in Fig. 3. The quality of dispersion and the percolation threshold can be deduced from this result. The conductivity is linear with $(v-v_c)$ on a logarithmic scale described by the equation:

$$\text{Log} \sigma = \text{Log} A + \text{Log}[(v - v_c)^t]$$

where σ is the conductivity of the nanocomposite, v is the volume fraction of the SWNT in the nanocomposite, v_c is the percolation volume fraction, A and t are fitted constants. A best fit to the data results when $A = 5 \times 10^{-2} \text{ S/cm}$ and $t = 1.71$, resulting in a $v_c = 0.04 \text{ vol\%}$. This fit is shown in the inset of Fig. 3. Fig. 4 shows the dielectric constant at different SWNT vol%. A high value is seen above the percolation threshold. The value increases until 0.5 vol% SWNT content above which the value plateaus off. The low percolation threshold quantifies the observation of excellent dispersion.

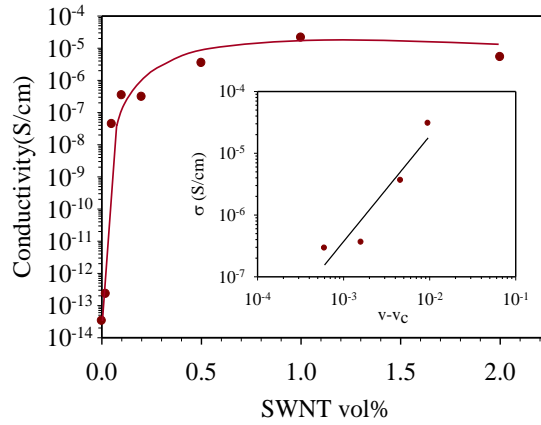


Fig. 3. Variation of conductivity with SWNT loading (The solid line in the main figure is added to ease the reading of the data; the solid line in the inset is the linear trend exhibited by the data).

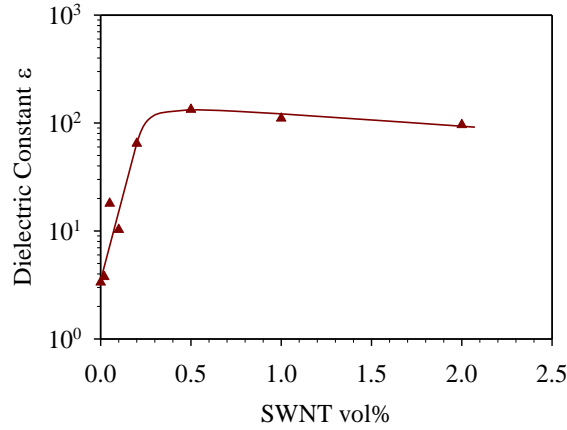


Fig. 4. Variation of Dielectric Constant with SWNT loading (The solid line is shown to ease the reading of the data).

Upon application of DC and AC electric fields to the series of nanocomposites, we observed both thickness and bending actuation. It is noted that nanocomposites below the percolation threshold do not show any significant actuation response, whereas samples above percolation exhibit both thickness and bending strains. For the thickness experiment (see Fig. 2(a)), the strains are calculated by the measured change in the thickness (Δt). S_{33} is the out-of-plane strain (3-direction) when the electric field is applied through the thickness (t). For the bending experiment, a sample strip with silver electrodes on both faces is suspended vertically as a cantilever with a voltage applied to both faces through the thickness. The length extensional strain resulting from bending is computed by modeling the bent strip as a cantilever beam under uniform load and assuming a constant radius of curvature (see Fig. 2(b)). The strains can then be computed using the S_{11} equation shown in previous section. The strain S_{11} is measured along the length (1-direction) due to an electric field applied through the thickness (3-direction). Thickness strains S_{33} for composites with 0.1vol%, 0.5vol%, 1vol% and 2vol% SWNT loadings are plotted in Figure 5. The data is collected at 1 Hz frequency. The strains increase non-linearly with the magnitude of electric field as seen in Fig. 5a. A striking observation is the low magnitude of electric fields required for actuation; the magnitude of the field is one to three orders lower than that required for other electrostrictive polymers like polyurethane [21] and poly(vinylidene fluoride-trifluoroethylene) [22]. We also see an enhancement in the actuation response as the SWNT

loading increases from 0.1 to 1vol%. At 2vol% SWNT loading however, the nanocomposite shows a decrease in strain compared to 1vol% SWNT loading sample. This is most likely due to the high conductive losses at high SWNT loadings. Fig. 5b confirms the dependence of the electromechanical strains on the square of the electric field, where the solid lines are linear fits with R^2 values in the range of 0.94 - 0.97.

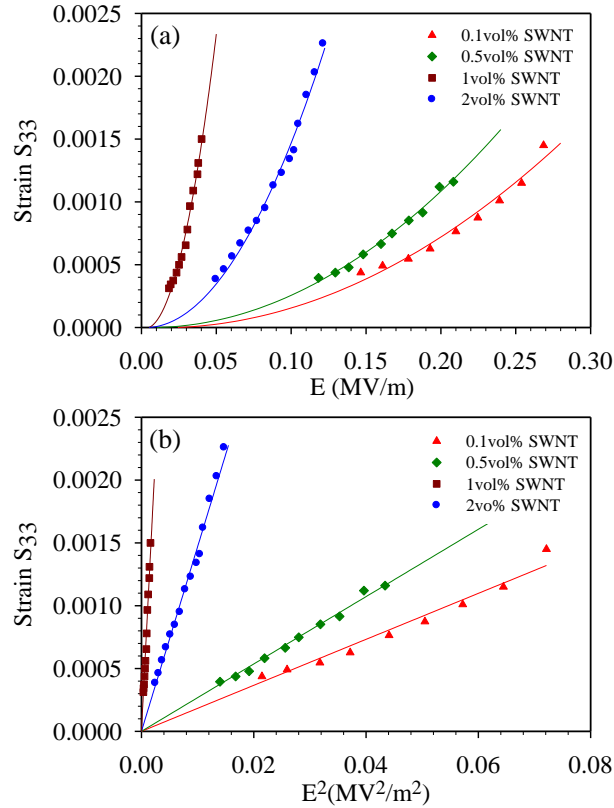


Fig. 5. (a) Thickness strains as a function of AC electric field (1Hz) and SWNT content. (b) Thickness strains proportional to squared electric field. Solid lines are quadratic fit for (a), and linear for (b).

Length extensional strains S_{11} for the composites under DC and AC fields are shown in Figures 6 and 7 respectively. Similar to thickness actuation, the electric field magnitudes required in the bending experiment are very low. Also, the strains are proportional to the square of the electric field as can be seen in Figs. 6b and 7b. Finally, the bending actuation response is higher as the SWNT loading increases up to 1vol%SWNT content, above which a decrease is seen due to conductive losses in the material.

We also investigated the strain rate, i.e., how quickly the strain reaches a maximum value under an applied electric field. Fig. 8 shows strain as a function of time at different DC voltages for 0.5vol% SWNT loading. The strain increases linearly after an initial lag of a few seconds, and then plateaus off. An increase in the strain rate is seen with an increase in the applied voltage. Similar observations are made at different vol% SWNT loading. The strain rate at 7V for 0.5vol% SWNT is greater than that for 0.1vol% SWNT at the same voltage; the thickness of samples was the same. Thus, the strain rate increases with increase in voltage and SWNT loading. These results are summarized in Table1.

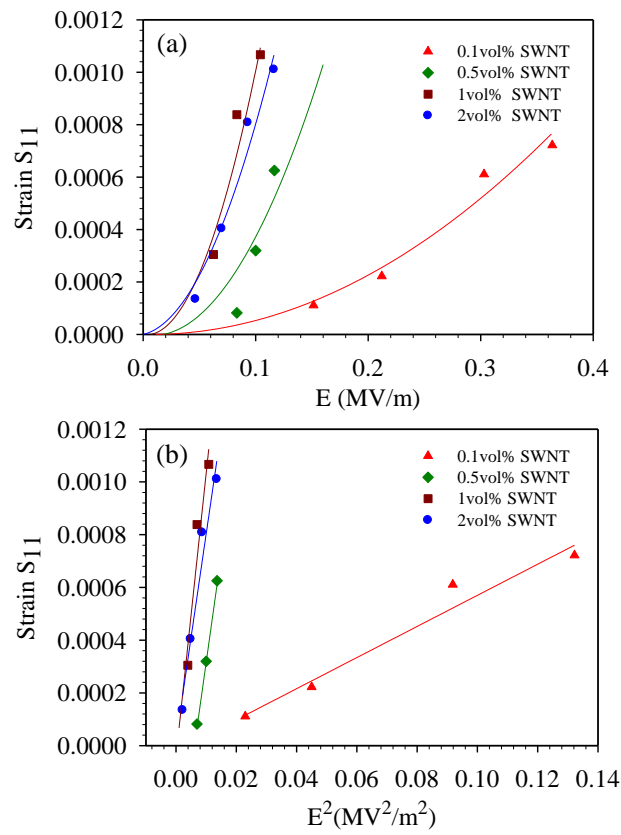


Fig. 6. (a) Length extensional strains as a function of DC electric field and SWNT content. (b) Length extensional strains proportional to squared electric field. Solid lines are quadratic fit for (a), and linear for (b).

Table 1 Strain rates at different SWNT content and applied voltages

Voltage (V)	Strain Rate (s ⁻¹)	
	0.1vol% SWNT	0.5vol% SWNT
5	-	4×10^{-6}
6	-	2×10^{-5}
7	4×10^{-5}	5×10^{-5}

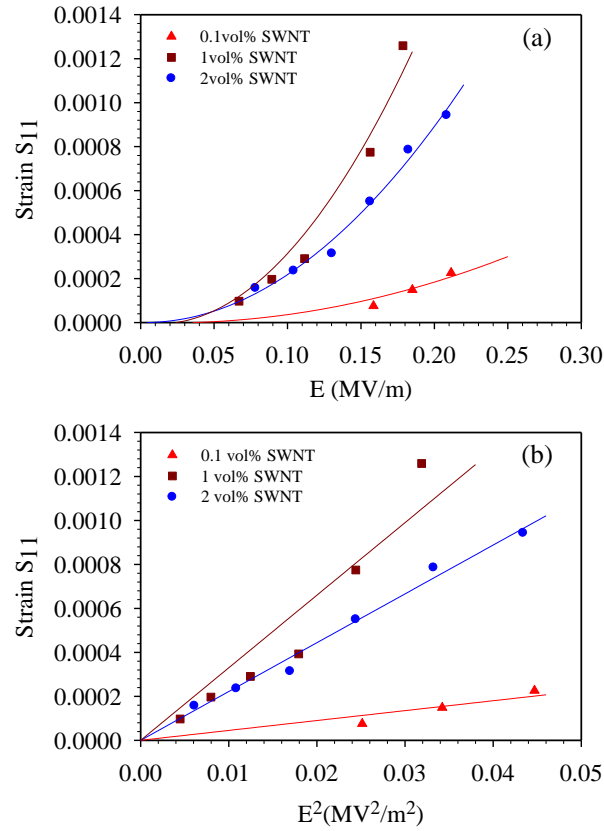


Fig. 7. (a) Length extensional strains as a function of AC electric field (0.5Hz) and SWNT content. (b) Length extensional strains proportional to squared AC electric field. Solid lines are quadratic fit for (a), and linear for (b).

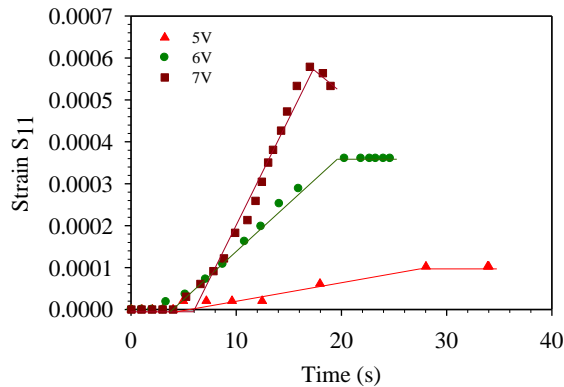


Fig. 8. Strain rates compared at different voltages for 0.5vol% SWNT+PI.

The strain data presented so far suggests a proportionality of the thickness and elongation strains with the square of the electric field, indicating a quadratic response. The quadratic response can also be observed physically in the bending case where the sample bends in the same direction after reversing the direction of the applied DC field, while for an AC field the sample bends in the same direction in the consecutive half cycles of the signal. A quadratic actuation response to an electric field could be due to three reasons: a) Electrostatic effect b) Joule heating and c)

Electrostriction. Electrostatic actuation can be ruled out as the mechanism driving the actuation response for the following reasons: (1) the polyimide is rigid since it is well below its glass transition temperature T_g , therefore the contributions from Maxwell stress are negligible. Our calculations indicate a maximum contribution from Maxwell strain of the order of 10^{-9} to 10^{-10} . (2) Electrostatic actuation leads to a decrease in thickness in response to applied field, whereas our samples show an increase in the thickness under the applied field. Similarly, electrostatic actuation in the cantilever experiment would cause a decrease in thickness due to Maxwell's pressure and would not result in bending. The next possibility is Joule heating. To account for strains due to Joule heating, the temperature of the faces of the films was measured under applied voltage using a thermocouple. The difference in temperature between the two faces of the film actuator was found to be negligible. Also, heating the actuator to the temperature detected by the thermocouple (when the sample is subjected to an electric field) in an oven showed no bending response. In a different study, it has been shown that the difference in the coefficient of thermal expansion between pure CP2-PI and SWNT+CP2-PI nanocomposites is negligible. Since the bending response is thought to result from the formation of resin rich and SWNT rich layers during film casting, the effect of non-uniform thermal expansion of the resin rich and SWNT rich layers due to Joule heating would be negligible. The final possibility we investigate is electrostriction. In electrostriction, the strain S_{ij} is related to the polarization vectors P_k and P_l through the electrostriction coefficient (Q_{ijkl}) as,

$$S_{ij} = Q_{ijkl} P_k P_l$$

For the case of linear dielectric materials, polarization can be expressed in terms of the electric field as,

$$P_i = \epsilon_0 (\epsilon_{ij} - 1) E_j$$

where ϵ_0 is the permittivity of free space ($=8.85 \times 10^{-12}$ F/m) and ϵ_{ij} is the permittivity of the dielectric material. Hence the electrostrictive strain can then be written in terms of the electric field vectors E_r and E_s as,

$$S_{ij} = M_{ijrs} E_r E_s$$

Where M_{ijrs} is the electrostriction coefficient related to the electric field. The two coefficients are related to each other through,

$$M_{ijrs} = \epsilon_0^2 (\epsilon_{kr} - 1) (\epsilon_{ls} - 1) Q_{ijkl}$$

The coefficient of electrostriction M_{3333} and M_{1133} can be calculated from the strain vs. squared electric field plots. Fig. 9 compares the coefficients for our composites with known electrostrictors like polyurethane and PVDF copolymer P(VDF-TrFE). M_{3333} at 1 Hz shows an increase with SWNT content up to 1vol% SWNT above which we observe a decrease in the value. Similarly an increase in the M_{1133} coefficient for the DC case up to 1vol% SWNT is observed, above which, the value plateaus off. Under AC field, the M_{1133} values are lower than in the DC case. In general, the coefficients of electrostriction for the SWNT-PI composites are six to eight orders higher than those demonstrated by electrostrictive Polyurethane [23] and PVDF-TrFE [22].

As mentioned earlier, both El-Hami et al. and Guo et al. have concluded that SWNTs exhibit an electrostrictive behavior [8,9]. However, the coefficient of electrostriction measured in [8] is a

low $2 \times 10^{-6} \text{ m}^2/\text{MV}^2$, which does not account for the high electrostrictive coefficient seen in Fig. 9. Since electrostriction is a polarization dependent phenomenon (Equation 4), results of TSC and dielectric relaxation experiments offer an explanation to this emergence and enhancement of the actuation response. Fig. 10(a) shows the depolarization current per unit area for 0.05 vol% SWNT-PI and 0.1 vol% SWNT-PI composites. The area under the peaks corresponds to the polarization induced in the composites. Inspection of Fig. 10a shows that the 0.1 vol% composite has a higher polarization as compared to the 0.05 vol% composite. Fig. 10(b) summarizes the polarization for three different samples: pure PI (CP2), 0.05vol% SWNT+PI and 0.1vol% SWNT+PI at the same poling temperature (glass transition of the system, which is around 200°C) but different poling fields. An increase is observed in the induced polarization with the SWNT content and poling field. Effect of poling temperature was also investigated and a higher polarization is also seen for poling temperatures closer to the glass transition temperature. Those results are not shown here.

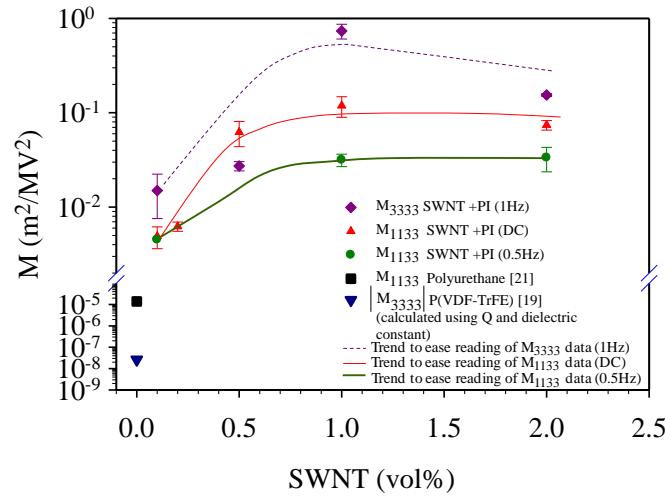


Fig. 9. Comparison of coefficients of electrostriction. Solid lines are drawn to ease the reading of the data.

The remnant polarization, polarization due to permanent dipole contributions, is given by the Clausius Mossotti equation [24]:

$$P_R = \Delta\epsilon \epsilon_0 E$$

where, ϵ_0 is the permittivity of free space, E is the applied electric field, and $\Delta\epsilon$ is the dielectric relaxation strength, which is the difference between the static (low frequency) and high frequency limits on dielectric constant. The $\Delta\epsilon$ value can also be measured by using temperature instead of frequency. The behavior of dipoles under high temperature is analogous to that at low frequency, while that at low temperature is analogous to the behavior at high frequency. Fig. 11 shows the increasing difference between the high and low temperature values of dielectric constant ($\Delta\epsilon$) for different SWNT loading at 21.5Hz. This value increases with SWNT loading as seen in Table 2, indicating an increase in the dipolar relaxation and remnant polarization with SWNT loading.

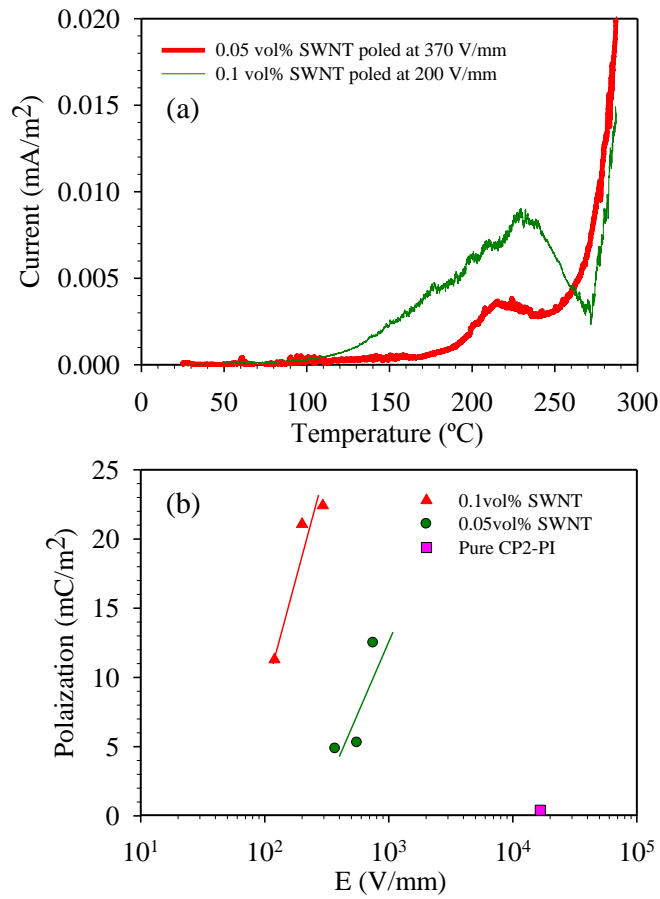


Fig. 10. (a) Depolarization current as a function of temperature for 0.05 vol% and 0.1 vol% SWNT samples, (b) Polarization induced in the nanocomposites by TSC with varying SWNT loading compared to pure polyimide. Solid lines are used to ease the reading of the data.

Table 2 $\Delta\epsilon$ as a function of SWNT loading

SWNT loading (Vol%)	$\Delta\epsilon_{21.5 \text{ Hz}}$
0	0.69
0.02	0.72
0.05	21
0.1	24

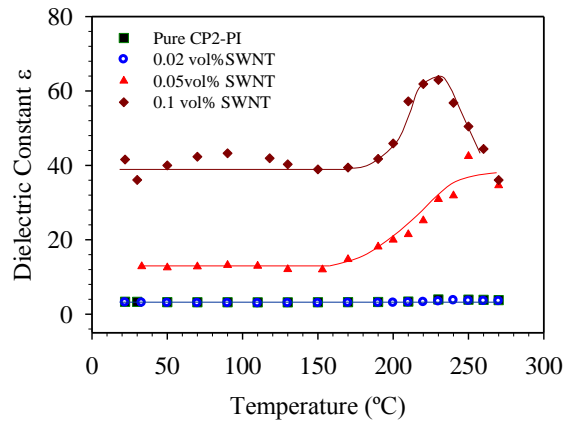


Fig. 11 Dielectric constant as a function of temperature at 21.5 Hz showing dipolar relaxation at different SWNT content.

Both Fig. 11 and Table 2 confirm the presence of dipolar polarization in the PI in the presence of SWNTs. Below, we propose some likely causes for the high polarization in the nanocomposite materials which in turn drives the electrostrictive response. The strain results suggest that the presence of SWNTs causes enhancement in polarization. The SWNTs used in this study are a mixture of metallic and semiconducting nanotubes, with a high effective dielectric constant [25-27]. This contrast in the dielectric constant between the SWNTs and the polymer can lead to accumulation of charges at the inclusion-polymer interface causing interfacial polarization [28]. Interfacial polarization increases with increase in the SWNT content and would explain the high dielectric constant values shown in Figure 4. However, contributions from dipoles inherent to the polymer matrix cannot be neglected. In our previous publication, we stated that the low percolation is thought to result from an electron hopping phenomenon called quantum tunneling, rather than from physical contact between the SWNTs [5]. Thus, presence of nano and micro-capacitors in between the SWNTs is possible. This conjecture is also supported by the increase in the dielectric constant of the nanocomposite with SWNT content (Fig. 4). Our calculations show that in a percolated SWNT structure a field up to 2 factors higher than the applied field could exist locally between SWNTs. In these calculations, SWNTs are assumed to be at random angles in the conducting path through the thickness of the nanocomposite films. The capacitors formed between the SWNTs are assumed to exist in series and the distance between the nanotubes is computed for a particular concentration using a concentric cylinder representative volume element. In CP2, the C-CF₃ bonds (Fig. 1) result in a dipole moment of around 2.95 debye [29,30] but due to the rigid dianhydride (6FDA) structure the movement of this dipole under an applied electric field is restricted. The higher local electric field between the SWNTs could cause the weak dipoles to rotate, contributing to the enhanced induced polarization. Enhanced polarization due to SWNT - PI interaction can also exist due to the presence of a secondary non-covalent interaction between the polymer and SWNTs, such as a donor-acceptor charge interaction between the CP2 and the SWNTs. Researchers have shown evidence of donor-acceptor interactions between SWNT and polymer dipoles [31,32]. These studies concluded such a relationship between SWNTs and polar polymers like (β-CN) APB-ODPA [31] and PVDF [32] through Raman and FTIR spectroscopy studies. A similar noncovalent relationship could also exist due to sharing of a π-electron between the aromatic molecules on the polymer chain and the SWNTs as suggested by [33,34]. Zhao et al. [33] have analyzed this noncovalent interaction using density functional calculations, while Chen et al. [34] have demonstrated this experimentally by engineering various composites using this interaction between the polymer and SWNTs. Thus an electron donor acceptor interaction between the SWNT and the electronegative

group on the polymer chain or due to adsorption of aromatic groups on to the SWNT can lead to a noncovalent interaction. Thus results point to contributions from three sources towards the enhanced actuation mechanism in the nanocomposite: the SWNTs acting as extended electrodes, interfacial polarization and the interaction between the polymer and the SWNTs. This interaction and resulting polarization can also cause the enhanced electrostrictive effect. More on interaction and mechanisms will be discussed in ‘Results-Section C’.

B. PVDF nanocomposite actuators as electrostrictors:

One significant finding in this area is that, through judicious selection of nanoparticles and polymers, we can tailor the electromechanical response of polymer-based nanocomposites. With increases in SWNT content and dipole moment of the polymer, the free-strain response of the polymer nanocomposites increases (Figure 12). The magnitude of electric field required for the actuation is in the range of 0.01-0.4 MV/m, which is significantly lower than that required to drive current electronic EAPs (see Table 3). This result demonstrates that we can manipulate the electric field required and the observed strain field to achieve it by choosing the nanoparticle content and the type of polymer matrix used. Figure 13 shows the coefficient of electrostriction M_{3333} for a number of nanocomposites systems we studied and compared to known electrostrictive polymer polyvinylidene trifluoroethylene P(VDF-TrFE) [35]. The coefficient is plotted as a function of SWNT vol% for a more direct comparison between the different systems.

Table 3. Comparison of actuation electric fields.

Polymer	Max Strain (%)	Applied Field (MV/m)	Ref.
PVDF +0.26 vol% SWNT	0.24	0.05	Our study
CP2 +2vol% SWNT	0.23	0.015	Our study
(β -CN)APB-ODPA+0.5 vol% SWNT	0.4	0.3	Our study
P(VDF-TrFE) Electrostrictor	4	150	Ref. 35
Piezoelectric PVDF	0.7 (calculated)	230	Ref. 36

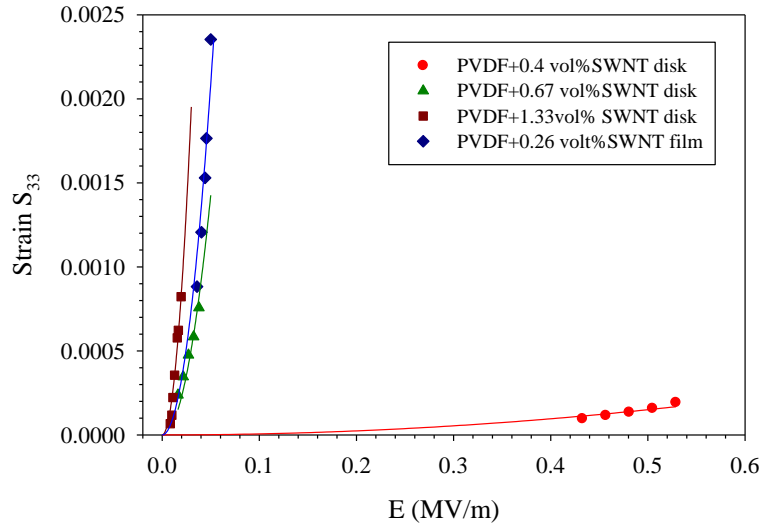


Fig 12. Thickness strains for PVDF nanocomposites

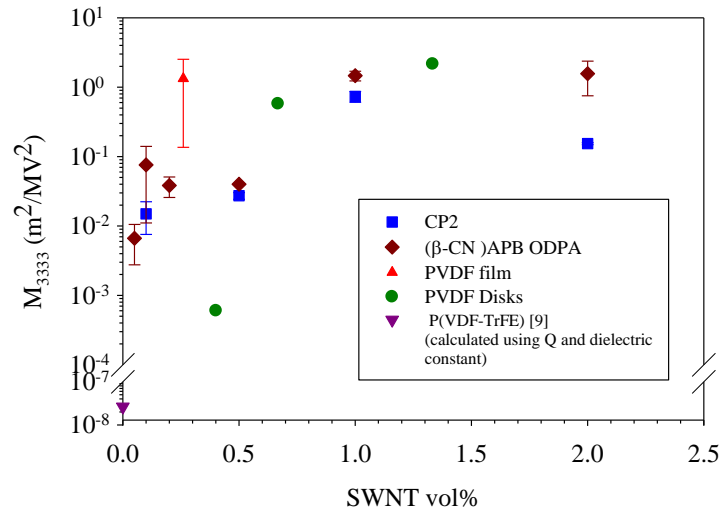


Fig 13. Comparison of coefficient of electrostriction for previously-studied polymer-based nanocomposite systems

C. Probing mechanism of electrostriction:

Our program probed experimental issues of understanding origins of enhanced piezoelectric and/or electrostrictive behavior of polymer nanocomposites.

The bending electrostrictive strains result from an inherent unimorph character of the nanocomposite films. This behavior also offers an insight into the mechanism driving the electrostrictive response. The inherent unimorph is created due to formation of a single walled carbon nanotube (SWNT) deficient layer near the glass surface on which the nanocomposite film is cast. The nanocomposite cast surface (film surface on the glass slide) is the SWNT deficient layer while the free surface is the SWNT rich layer. Figure 14 shows the bending response resulting from the inherent unimorph character.

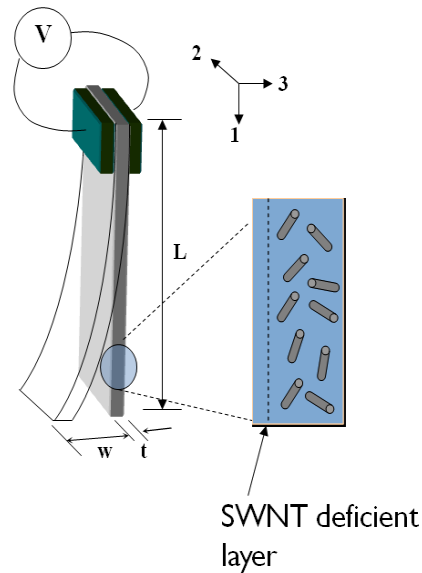


Fig 14. Bending electrostriction due to inherent unimorph

Conductive atomic force microscopy (C-AFM) is used to confirm the formation of SWNT deficient and SWNT rich layers. Figure 15 shows the C-AFM mapping of the cast and free surface of a 2%SWNT – CP2 film. From the figure it can be observed that the free surface reveal a higher concentration of current carrying SWNTs in response to an applied voltage. The cast surface however shows a much lower content of SWNTs thus confirming the unimorph character of the films.

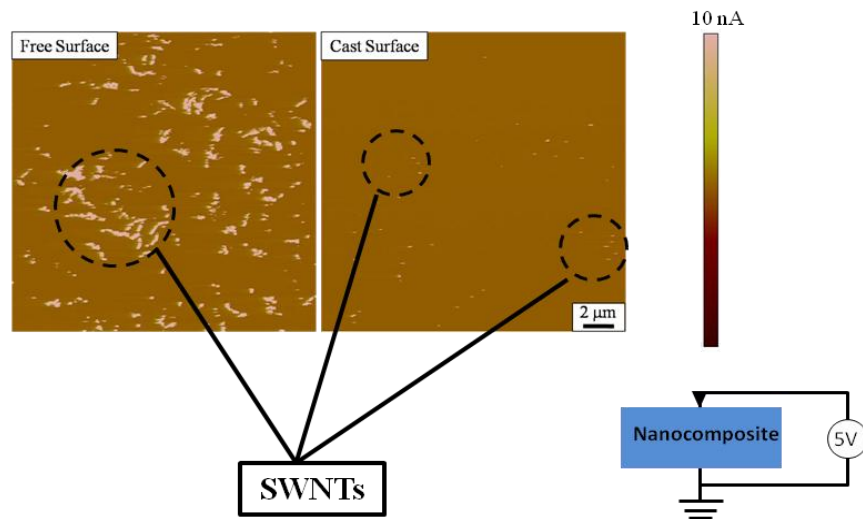


Fig 15. Conductive AFM mapping of the cast and free surfaces of 2%SWNT-CP2 film

The SWNT rich layer (free surface) acts as the active layer in the unimorph while the SWNT deficient layer (cast surface) acts as the constraining layer. The active layer of the nanocomposite unimorph expands in thickness that can also be confirmed by the thickness actuation experiments.

Presence of SWNTs also results in enhanced polarization. Figure 16 shows the dielectric constant as a function of frequency for PVDF nanocomposites with varying SWNT content. In general the dielectric constant increases with SWNT content indicating an enhanced polarization due to SWNTs. Similar observations are also made for SWNT-CP2 composites.

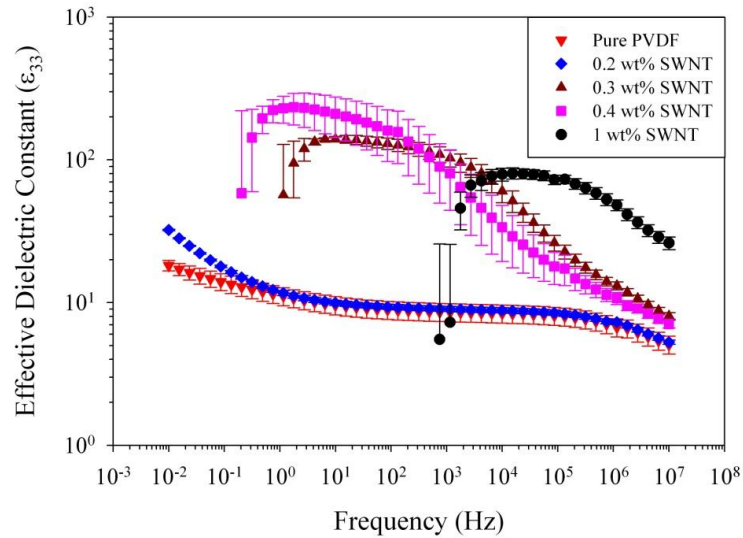


Fig 16. Effective dielectric constant vs frequency at different SWNT loading

The electrostrictive strains in the active layer results from enhanced polarization due to;

1. SWNTs acting as extensions of electrodes
2. Interfacial and induced polarization
3. Formation of a polar microstructure (for polyvinylidene fluoride (PVDF) composites)
4. Joule heating

1. SWNTs acting as extension of electrodes. The nanocomposite films demonstrate an actuation response at around the percolation threshold. At the percolation threshold the SWNTs form a network where electrical conductivity occurs due to an electron-hopping phenomenon. However, since the SWNTs are not physically connected to each other they also form micro or nano-capacitors locally which can see as much as an order higher electric field than that applied to the composite. This enhanced local electric field can result in high polarization in the nanocomposite films resulting in the enhanced electrostrictive effect. Figure 17 shows a schematic of the enhanced local electric field due to presence of SWNTs.

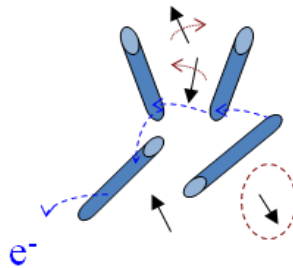


Fig 17. Enhanced polarization due to micro or nano-capacitors

2. Interfacial and induced polarization. The contrast in the dielectric and electrical properties of SWNTs and the polymer matrix also results in interfacial polarization at the interfaces between SWNTs and the polymer matrix. The SWNTs can also form a secondary non-covalent interaction with the electronegative groups on the polymer chains. These scenarios are depicted in Figure 18 (a) and (b) respectively. The presence of SWNTs can thus result in enhanced interfacial and induced polarization.

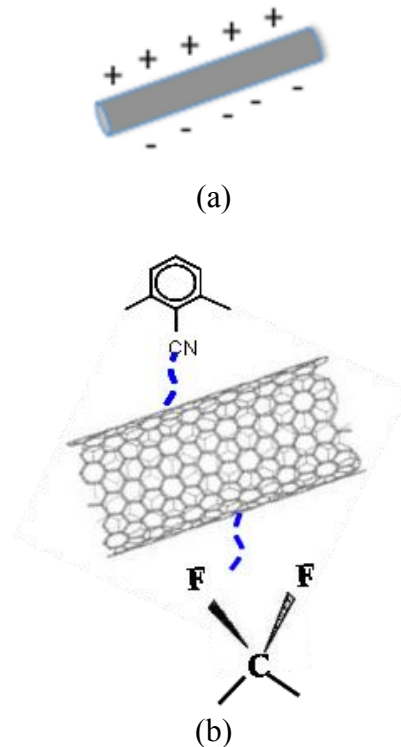


Fig 18. (a) Interfacial and (b) induced polarization

3. Formation of a polar microstructure. In polymorphic polymers like polyvinylidene fluoride (PVDF), presence of SWNTs can also transform a non-polar phase to a polar phase. PVDF is typically in a non-polar α phase if it is un-stretched and un-poled and hence it does not demonstrate any electromechanical response. However in the presence of SWNTs the non-polar α phase is transformed to polar γ phase. Figure 19 shows the Fourier transform infrared spectroscopy (FTIR) scans of SWNT-PVDF nanocomposites. It can be seen that the non polar α phase microstructure is converted to a polar γ phase due to the presence of SWNTs. Thus formation of a polar microstructure coupled with the SWNTs forming micro or nanoc-capacitors would result in enhanced polarization and an electrostrictive effect. Figure 20 summarizes this scenario.

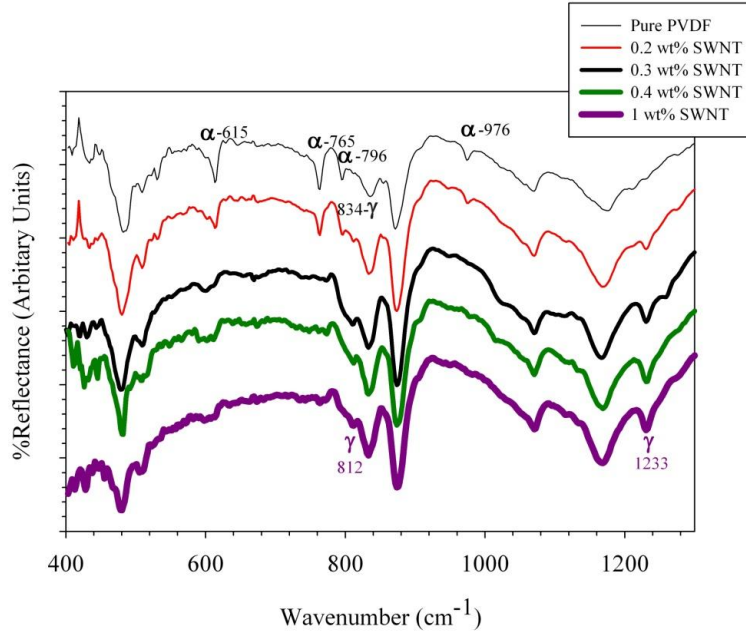


Fig 19. FTIR results for PVDF nanocomposites

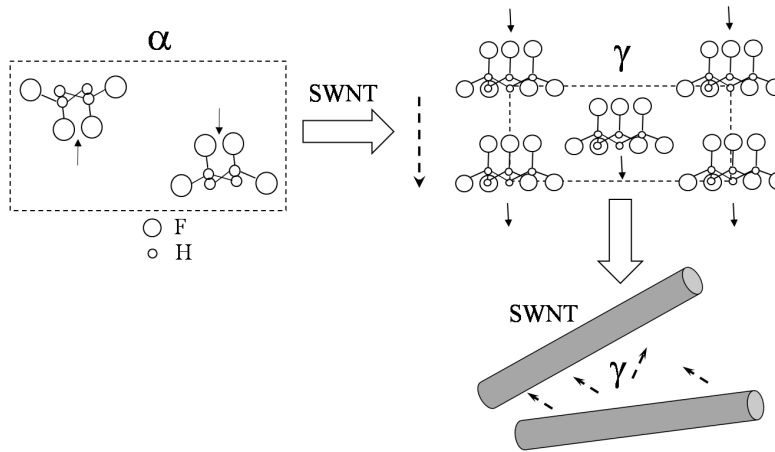


Fig 20. Polarization due to formation of polar γ phase by adding SWNTs.

4. Joule Heating. Ultimately the quadratic electromechanical response can also result from Joule heating. Figure 21 shows the increase in temperature of the nanocomposites with the 1 Hz AC sinusoidal electric field measured using a contact thermocouple. From Figure 21 it can be inferred that the temperature rise in the 0.3 wt% SWNT and 0.4 wt% SWNT samples is very minimal. The temperature rise at the electric fields that caused thickness actuation for these nanocomposites was less than 0.5 °C. An Infrared IR temperature gun also showed comparable temperature change data. The conductive 1 wt% SWNT samples however did show a temperature increase of about 4°C. Since PVDF is already above the glass transition temperature (T_g) at room temperature (T_g for PVDF is -35°C) Joule heating can have a possible contribution towards the strain response of 1% SWNT content samples. Figure 22 (a) shows the projected Joule heating contributions of 1wt% SWNT samples using the temperature increase data and the coefficient of thermal expansion (1.1×10^{-4} /°C, measured using the thermo mechanical analyzer (TMA)).

Figure 22 (b) shows the corrected M_{33} coefficient for the 1wt% SWNT data. The Joule heating contributions to the measured strain response were not significant. Though potentially minimal, the Joule heating contributions need to be systematically studied by more precise techniques of temperature measurements like infrared thermal imaging.

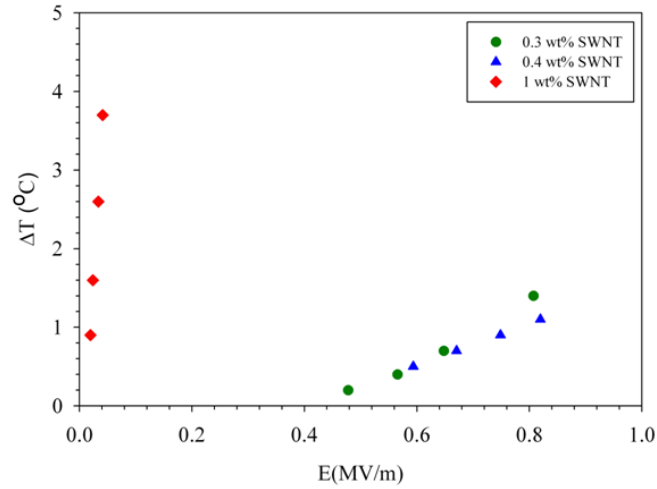


Fig 21. Temperature increase in PVDF nanocomposites due to Joule heating at 1 Hz

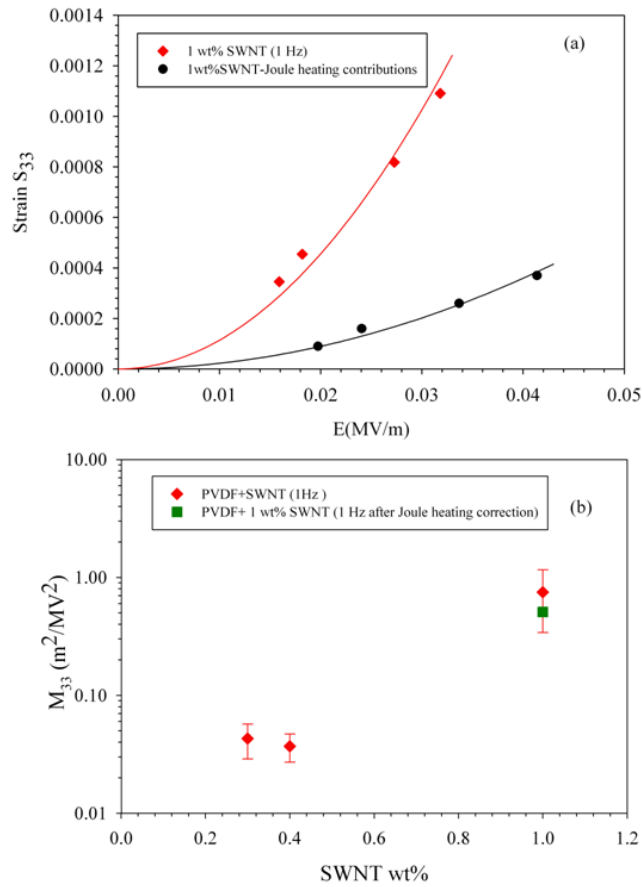


Fig 22. (a) Joule heating contributions to strain response of 1wt% SWNT+PVDF composites (b) M_{33} value for 1wt% SWNT+PVDF after Joule heating correction compared with measured M_{33}

D. Summary of significant findings

In this project, we show that adding single walled carbon nanotubes (SWNTs) to a non-actuating polyimide (PI) results in an electromechanical actuation response in the nanocomposite. The neat polyimide does not show any actuation response under an applied electric field, whereas the SWNT-PI composites above the percolation threshold exhibit an electrostrictive behavior that is highly dependent on SWNT content. Both bending and thickness-extension strains are obtained at very low electric field magnitudes; the study also evaluates the effect of applied electric field magnitude, frequency and SWNT content on the actuation strain and strain rate. Dielectric spectroscopy and thermally stimulated current measurements reveal an enhanced polarization in the presence of SWNTs. This enhancement is key to the actuation mechanism and is thought to arise from a combination of three sources: SWNTs acting as extended electrodes within the polymer, interfacial polarization and noncovalent interactions between the SWNTs and the polymer. Similarly, we also study investigated the effect of SWNTs on the electromechanical properties of PVDF. PVDF+SWNT samples show an enhanced quadratic electromechanical response, which is absent in the pure PVDF and increases with increasing SWNT content. DSC and FTIR results indicate that the percentage crystallinity remains the same upon addition of SWNTs, but presence of SWNTs converts the non-polar α phase into the polar γ phase. The nanocomposite samples also demonstrate an enhancement in the dielectric constant as compared to the pure PVDF. Finally, despite the fact that PVDF is above its T_g at room temperature, possible contributions from Maxwell's stress are orders of magnitude lower than the measured strains. Thus, the measured electromechanical response in the PVDF+SWNT nanocomposites results from enhanced induced polarization and is believed to be electrostrictive. Finally the contributions from Joule heating to the electromechanical strains are also probed but were not significant at the weight content investigated.

IV. DURIP Equipment-Enabled Research

Mechanical reliability is an important factor in designing as well as characterizing multifunctional materials. Different characterization techniques are used to investigate mechanical integrity of the structure under load. Scanning Electron Microscopy (SEM) and Transmission Electron Microscopy (TEM) are the most common methods to investigate fracture mechanism as well as crack propagation in addition to other microscopic phenomena at region of failure. However, microscopy techniques usually need extensive sample preparation procedures. They also cannot provide quantitative analysis of fracture mechanism in the sample. There is a great need for a more quantitative study of materials behavior under load.

A. Nano-indentation

Nano-indentation is a relatively new mechanical characterization technique that has been shown to be efficient in studying materials' mechanical behavior at the nanoscale. Nano-indentation can be considered as a nano hardness test. A nano-indenter (Figure 23) applies plastic deformation on the surface of a sample by applying a force. The height of penetration is monitored as well as the amount of force applied to the sample. The results of the test would be a force-height diagram which can be converted to mechanical properties of the sample like elastic modulus and hardness (Figure 24). One of the advantages of nano-indentation is the ability to apply nanoscale deformation on the sample. Nano-indentation increases the accuracy to apply local deformation at the nanoscale and detect the in-situ behaviour of nanocomposites in different regions of the material. Lee et. al. investigated mechanical properties of a cellulose fiber reinforced polymer nanocomposite by doing an array of nanoindentation in different regions of the sample. They showed how mechanical properties of different regions in the sample can be differentiated by aid of nanoindentation. Figure 25 shows a schematic view of their experiment. By accurate

positioning of the nano-indenter, starting from the fiber area, moving to the interphase and finally reaching the matrix, they were able to measure Hardness as well as Modulus values of the fiber and polymer as well as those of the interphase region (Figure 26).

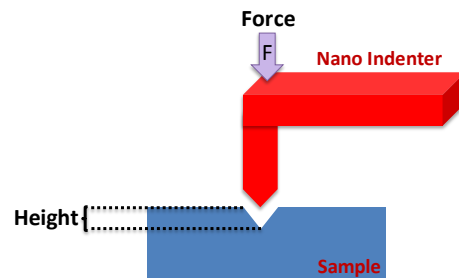


Fig 23. A schematic view of Nano-indentation test

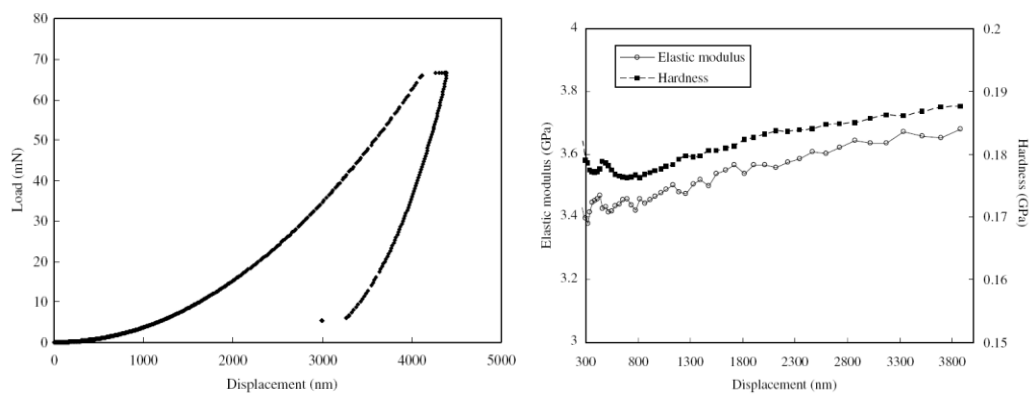


Fig 24. (left) Load (mN) (right) Elastic modulus and Hardness versus Displacement result of a nanoindentation test.

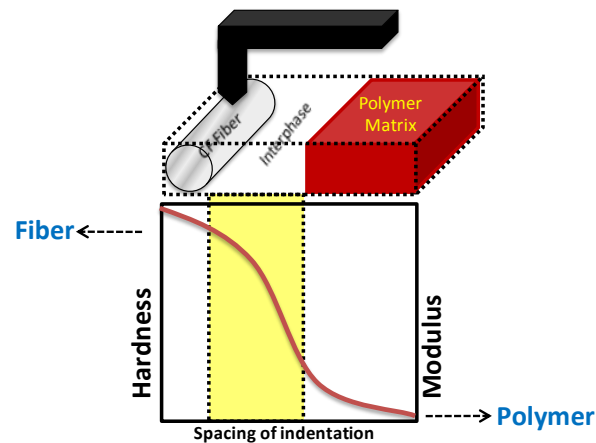


Fig 25. An schematic view of Lee et. al. Nanoindentation experiment

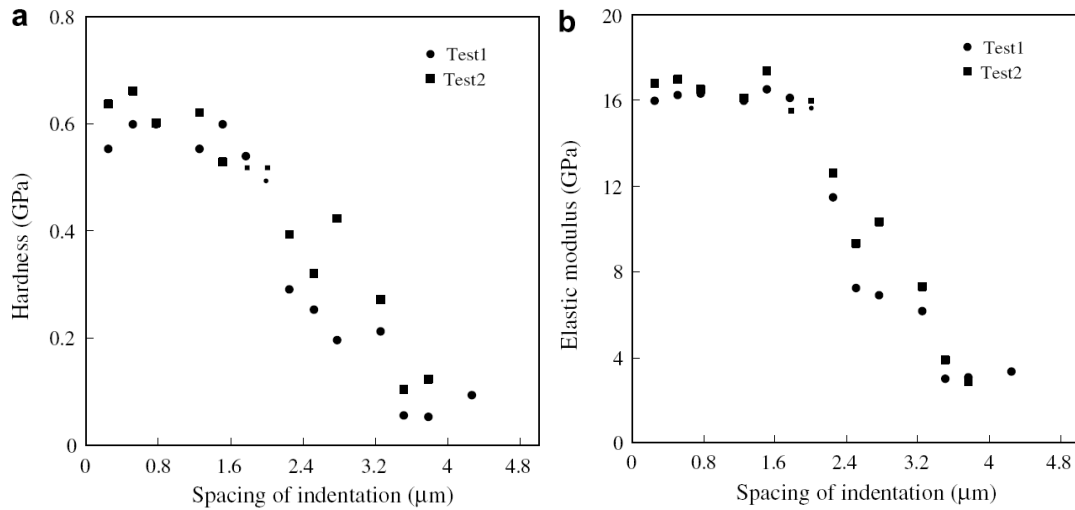


Fig 21- (Left) Hardness (right) Elastic Modulus as a function distance

B. Raman spectroscopy

Raman spectroscopy is one of the most powerful spectroscopy techniques to characterize various properties of CNTs and CNT based polymer nanocomposites. The non-invasive nature of Raman experiment as well as convenience usage and the ability to be combined with other techniques makes it a very useful characterization technique in CNT based polymer nanocomposites. In Raman spectroscopy, a sample is illuminated by a light source of single frequency and the scattered light is collected by an optical sensor. The difference between the energy of the incident light and the scattered light is the energy difference between the ground state and the excited state of the molecule and is plotted as the intensity versus Raman shift (wavenumber) of the sample (Figure 27).

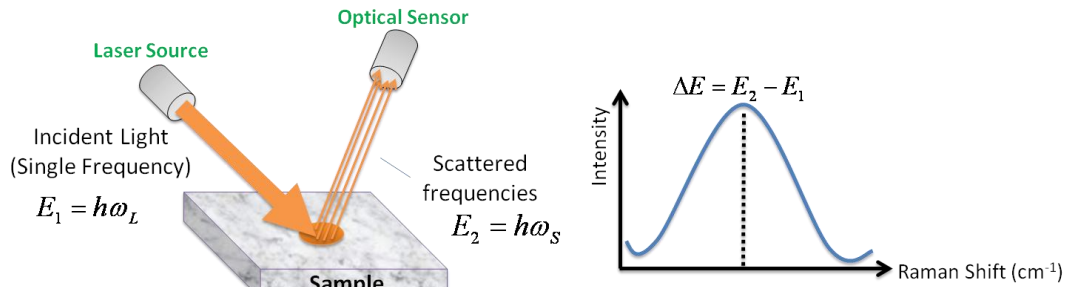


Fig 22- Raman Spectroscopy (A schematic view)

C. In-situ Raman combined with mechanical tests

Raman spectroscopy has been combined with other techniques to investigate Raman behavior of CNTs under applied mechanical deformations. Swan et. al. used atomic force microscopy (AFM) and stretched a single wall carbon nanotube (SWNT) by aid of an AFM tip. In the meanwhile they took Raman spectrum of the stretched SWNT by focusing Raman laser on it.

As can be seen in the Figure 28, after stretching SWNT, Raman peaks shift to lower wavenumbers. By this study, Swan et. al. were able to prove that Raman spectrum of CNTs is sensitive to mechanical deformation and this mechanical deformation, here CNTs elongation, can be characterized by Raman spectroscopy.

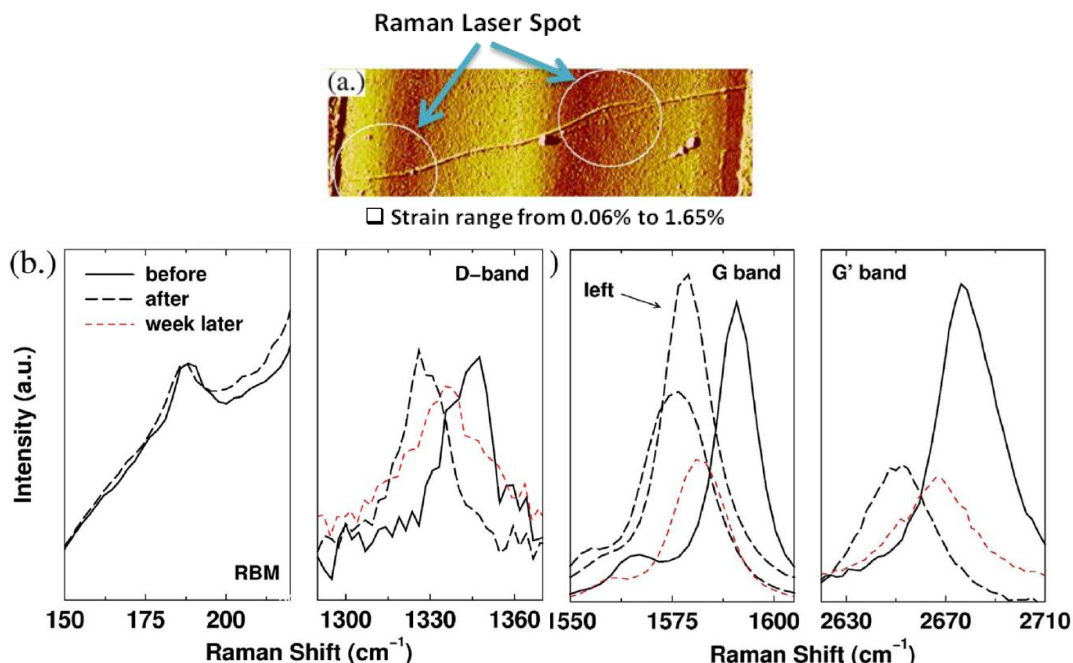


Fig 28. (Top) Raman Laser spot on stretched SWNT by AFM (Bottom) Raman Spectrum of SWNT before and after stretching by AFM tip.

D. *In-situ Raman spectroscopy/nano-indentation experiments*

In this study we proposed the idea of combining Raman spectroscopy and Nano-Indentation with the aim of characterizing mechanical deformation of the CNT/PVDF nanocomposite. Figure 29 shows three different scenarios that might happen when a CNT/PVDF sample is nanoindented.

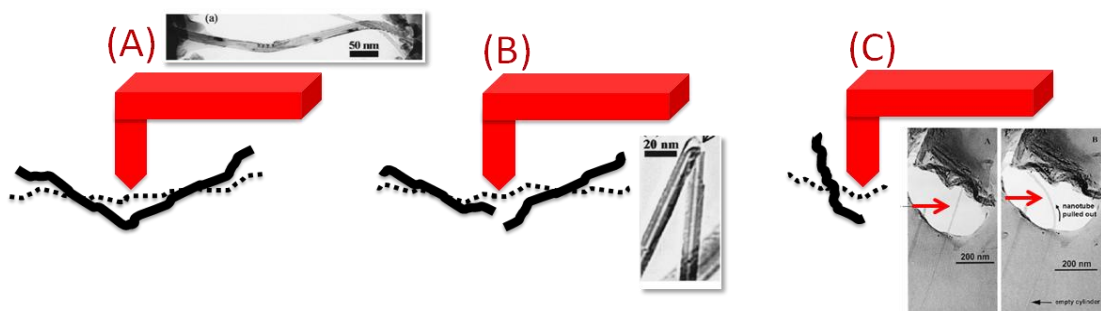


Fig 29. Three different failure mechanism scenarios of Raman Spectroscopy/Nano-Indentation experiment (A) Elastic deformation of CNT inside matrix (B) Breaking CNT in the matrix and (C) CNT pull out from the matrix

In the first scenario (A), elastic deformation of the CNT in the matrix is considered. In this case, CNT is either stretched, compressed or bent under Nanoindentation test. It is expected that a Raman shift would be observed upon nanoindentation. In the second scenario (B), Nanoindentation is beyond the elongation at break of the CNTs and causes CNTs to break under load. In this case, a Raman shift should be observed before breaking the CNTs. But promptly after CNTs break, Raman shift should return to its original position. In the last scenario (C), CNTs would be pulled out from the matrix. In this case interfacial bonding between CNTs and the PVDF is not strong and Nano-indentation simply separates the CNTs from the matrix. In this case, no Raman shift is expected to be observed.

E. Experimental procedure

Figure 30 schematically shows the experimental setup of in-situ Raman/Nano-Indentation experiment used in this study. The experiment was done in three major steps:

Step 1- Raman Spectroscopy of the sample

Step 2- In-situ Raman while Nano-indenting the sample

Step 3- Raman Spectroscopy of the indented area after Indentation

Nanoindentation was done in different indentation depths from 40 to 200nm in 40nm increments.

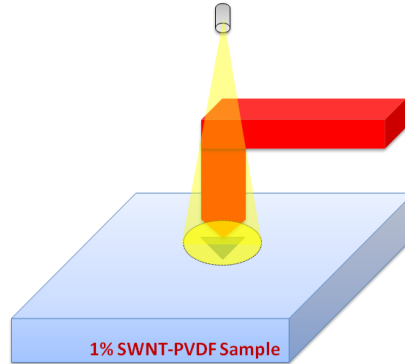


Fig 30. A schematic view of the in-situ Raman/Nano-indentation setup

F. Results and discussion

Raman Spectrum of SWNT in bulk besides SWNT embedded in PVDF are shown in Figure 31. As it seen in the Figure 31, there is an increase in wavenumber of all three major CNT bands after embedding in PVDF. This increase in Raman shift is a good sign of interaction and interfacial strength between SWNTs and PVDF polymer.

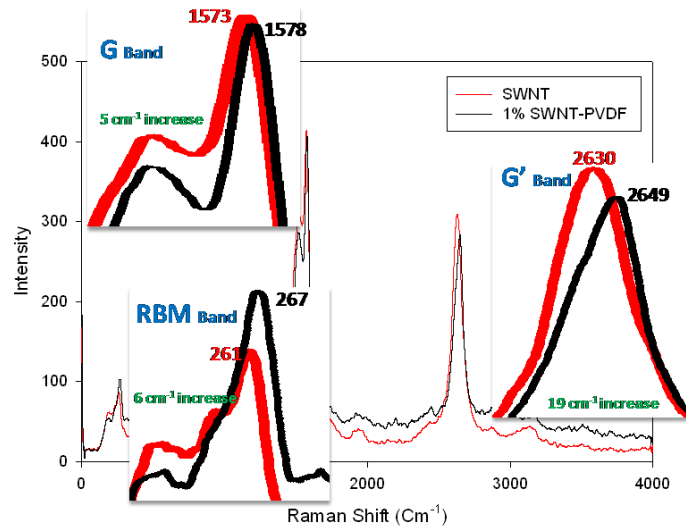


Fig 31. Raman Spectroscopy, SWNTsand SWNT-PVDF Nanococomposite

Figure 32 shows in-situ Raman/Nano-Indentation results in 120nm indentation depth. RBM and G-band didn't show any sensitivity to Nano-indentation. However G' band showed increase in Raman shift of the SWNTs after doing Nanoindentation.

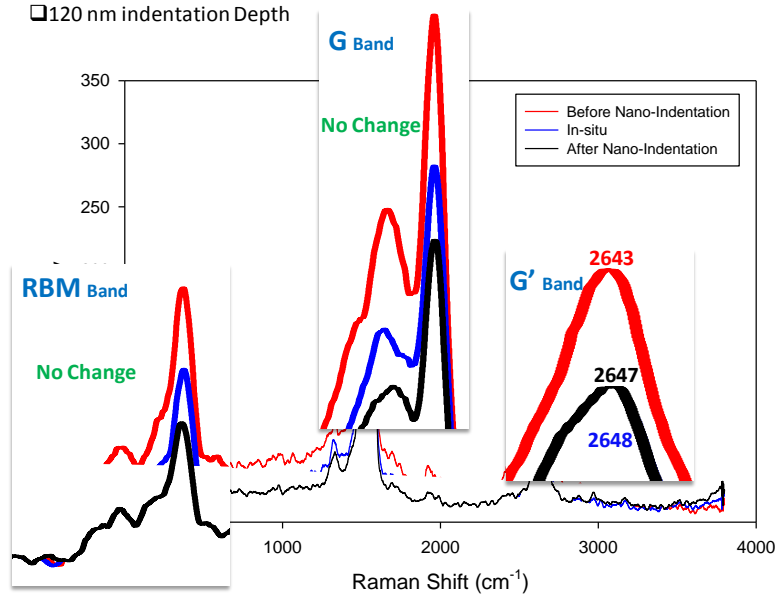


Fig 32. In-situ Raman/Nano-indentation results in 120nm indentation depth

Our results are also presented in Figure 33 for the Raman shift change as a function of indentation depth. It can be seen that there is an increasing trend by going to higher indentation depths. The highest Raman shift was observed in 120nm which can be a sign of highest indentation depths. After 120nm the Raman shift started decreasing. It can be argued that in indentations higher than 120nm, SWNTs undergo beyond deformation at break and cannot hold any more deformation. This causes SWNTs to break and as a result a decrease in Raman shift is observed.

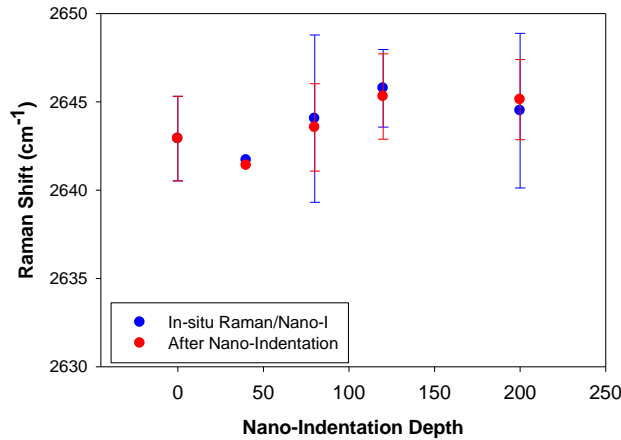


Fig 33. Raman Shift (cm^{-1}) as a function of Nano-indentation depth

V. Remaining Challenges

Despite these promising results and accomplishments, issues regarding designing desired actuator/sensor devices and optimizing their efficiency remain to be solved. In this context, understanding the origin of the electromechanical conversion in such polymer-based nanomaterials is crucial prior to addressing inefficiencies and developing device concepts. As a next step, we propose to target the remaining challenges using a combination of processing, experimental characterization and device modeling to help transition these materials technologies in a wide range of devices and applications.

REFERENCES

- [1] G. Zhou, W. Duan, B.L. Gu, First-principle study on morphology and mechanical properties of single-walled carbon nanotube, *Chem. Phys. Lett.* 333 (5) (2001) 344-349.
- [2] S.J. Tans, M.H. Devoret, H. Dai, A. Thess, R.E. Smalley, L.J. Geerligs, C. Dekker, Individual single-wall carbon nanotubes as quantum wires, *Nature* 386 (1997) 474-477.
- [3] L. Valentini, J. Biagiotti, J.M. Kenny, M.A. López Manchado, Physical and mechanical behavior of single-walled carbon nanotube/polypropylene/ethylene-propylene-diene rubber nanocomposites, *J. Appl. Polym. Sci.* 89 (2003) 2657-2663.
- [4] A. Dufresne, M. Paillet, J.L. Putaux, R. Canet, F. Carmona, P. Delhaes, S. Cui, Processing and characterization of carbon nanotube/poly(styrene-co-butyl acrylate) nanocomposites, *J. Mater. Sci.* 37 (2002) 3915-3923.
- [5] Z. Ounaies, C. Park, K.E. Wise, E.J. Siochi, J.S. Harrison, Electrical properties of single wall carbon nanotube reinforced polyimide composites, *Compos. Sci. Technol.* 63 (11) (2003) 1637-1646.
- [6] S. Roth, R.H. Baughman, Actuators of individual carbon nanotubes, *Curr. Appl. Phys.* 2 (4) (2002) 311-314.
- [7] R.H. Baughman, C. Cui, A.A. Zakhidov, Z. Iqbal, J.N. Barisci, G.M. Spinks, G.G. Wallace, A. Mazzoldi, D. De Rossi, A.G. Rinzier, O. Jaschinski, S. Roth, M. Kertesz, Carbon nanotube actuators, *Science* 284 (1999) 1340-1344.
- [8] K. El-Hami, K. Matsushige, Electrostriction in single-walled carbon nanotubes, *Ultramicroscopy* 105 (2005) 143-147.
- [9] W. Guo, Y. Guo, Giant axial electrostrictive deformation in carbon nanotubes, *Phys. Rev. Lett.* 91 (11) (2003).
- [10] J.H. Kang, C. Park, S.J. Gail, S.E. Lowther, J.S. Harrison, The effect of single wall carbon nanotubes on the dipole orientation and piezoelectric properties of polymeric nanocomposites, *NANO: Brief Reports and Reviews* 1 (1) (2006) 77-85.
- [11] N. Levi, R. Czerw, S. Xing, P. Iyer, D.L. Carroll, Properties of polyvinylidene difluoride-carbon nanotube blends, *Nano Lett.* 4 (7) (2004) 1267-1271.
- [12] S. Courty, J. Mine, A.R. Tajbakhsh, E.M. Terentjev, Nematic elastomers with aligned carbon nanotubes: new electromechanical actuators, *Europhys. Lett.* 64 (5) (2003) 654-660.
- [13] D.Y. Lee, I.-S. Park, M.-H. Lee, K.J. Kim, S. Heo, Ionic polymer-metal composite bending actuator loaded with multi-walled carbon nanotubes, *Sensor. Actuat. A-Phys.* 133 (2007) 117-127.
- [14] B.J. Akle, D.J. Leo, Single-Walled Carbon Nanotubes - Ionic Polymer Electroactive Hybrid Transducers, *J. Intel. Mat. Syst. Str.* 00 (2008) 1-11.
- [15] S. Zhang, N. Zhang, C. Huang, K. Ren, Q. Zhang, Microstructure and electromechanical properties of carbon nanotube/poly(vinylidene fluoride-trifluoroethylene-chlorofluoroethylene) composites, *Adv. Mater.* 17 (2005) 1897-1901.
- [16] C. Park, Z. Ounaies, K.A. Watson, R.E. Crooks, J.J. Smith, S.E. Lowther, J.W. Connell, E.J. Siochi, J.S. Harrison, Dispersion of single wall carbon nanotubes by in situ polymerization under sonication, *Chem. Phys. Lett.* 364 (2002) 303-308.
- [17] Dillon A C, Gennett T, Jones K M, Allenman J L, Parilla A and Heben M J 1999 A simple and complete purification of single-walled carbon nanotube materials *Adv. Mater.* **11** 1354 – 8.
- [18] Deshmukh S J and Ounaies Z 2009 Single Walled Carbon Nanotube (SWNT)-Polyimide Nanocomposites as Electrostrictive Materials *Sensor. Actuat. A-Phys.* **155** 246-52.

- [19] Nakagawa K and Ishida Y 1973 Annealing effects in poly(vinylidene fluoride) as revealed by specific volume measurements, differential scanning calorimetry, and electron microscopy *J Polymer Sci. Polymer Phys. Ed.* **11** 2153-71.
- [20] Benz M and Euler W B 2003 Determination of crystalline phases of poly(vinylidene fluoride) under different preparation conditions using differential scanning calorimetry and infrared spectroscopy *J. Appl. Polym. Sci.* **89** 1093-100.
- [21] M. Watanabe, M. Yokoyama, T. Ueda, T. Kasazaki, M. Hirai, T. Hirai, Bending deformation of monolayer polyurethane film induced by an electric field, *Chem. Lett.* (8) (1997) 773-774.
- [22] Q.M. Zhang, V. Bharti, X. Zhao, Giant Electrostriction and relaxor ferroelectric behavior in electron irradiated poly(vinylidene fluoride-trifluoroethylene) copolymer, *Science* **280** (1998) 2101-2104.
- [23] F.M. Guillot, E. Balizer, Electrostrictive effect in polyurethanes, *J. Appl. Polym. Sci.* **89** (2003) 399-404.
- [24] B. Hilczer, J. Malecki, *Electrets*; studies in electrical and electronic engineering, Vol. 14, Elsevier, New York, 1989, pp. 19.
- [25] L.X. Benedict, S.G. Louie, M.L. Cohen, Static polarizability of single-wall carbon nanotubes, *Phys. Rev. B* **52** (11) (1995) 8541-8549.
- [26] R. Krupke, F. Hennrich, H.V. Löhneysen, M.M. Kappes, Separation of metallic from semiconducting single walled carbon nanotubes, *Science* **301** (2003) 344-347.
- [27] J. Li, Q. Zhang, N. Peng, Q. Zhu, Manipulation of carbon nanotubes using AC dielectrophoresis, *Appl. Phys. Lett.* **86** (15) (2005).
- [28] P. Hedvig, *Dielectric spectroscopy of polymers*, John Wiley and Sons, 1977, pp. 293.
- [29] J.A. Dean, *Lange's handbook of chemistry*, McGraw-Hill INC, 1999, pp. 4.55.
- [30] J.A. Hinkley, J.F. Dezer, Crystallization of stretched polyimides: a structure property study, Vol. 301, NASA langley research center, NASA/TM-2002-211418 (2002).
- [31] K.E. Wise, C. Park, E.J. Siochi, J.S. Harrison, Stable dispersion of single walled carbon nanotubes in polyimide: the role of noncovalent interactions, *Chem. Phys. Lett.* **391** (2004) 207-211.
- [32] F.J. Owens, J.R.P. Jayakody, S.G. Greenbaum, Characterization of single walled carbon nanotube: Polyvinylidene difluoride composites, *Compos. Sci. Technol.* **66** (2006) 1280-1284.
- [33] J. Zhao, J.P. Lu, J. Han, C.-K. Yang, Noncovalent functionalization of carbon nanotubes by aromatic organic molecules, *Appl. Phys. Lett.* **82** (21) (2003) 3746-3748.
- [34] J. Chen, R. Ramasubramaniam, C. Xue, H. Liu, A versatile, molecular engineering approach to simultaneously enhanced, multifunctional carbon-nanotube-polymer composites, *Adv. Funct. Mater.* **16** (1) (2006) 114-119.
- [35] Zhang, Q.M., Bharti, V., Zhao, X., "Giant Electrostriction and relaxor ferroelectric behavior in electron irradiated poly(vinylidene fluoride-trifluoroethylene) copolymer", *Science*, **280**, pp.2101-2104, 1998.
- [36] Jow, T.R., Cygan, P.J., "Dielectric breakdown of polyvinylidene fluoride and its comparisons with other polymers", *Journal of applied physics*, **73**, (10), pp.5147-5151, 1993.